

# Thiol Ligand-Modified Au for Highly Efficient Electroreduction of Nitrate to Ammonia

Yuheng Wu, Xiangdong Kong, Yechao Su, Jiankang Zhao, Yiling Ma, Tongzheng Ji, Di Wu, Junyang Meng, Yan Liu,\* Zhigang Geng,\* and Jie Zeng\*

Cite This: <https://doi.org/10.1021/prechem.3c00107>

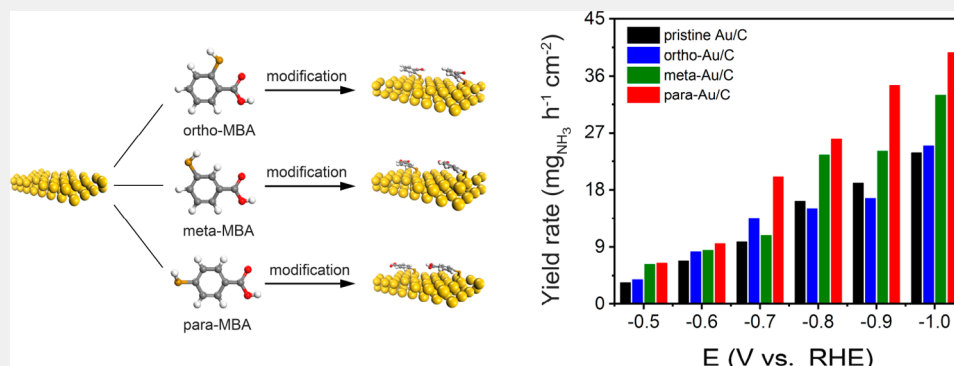
Read Online

ACCESS |

Metrics & More

Article Recommendations

Supporting Information



**ABSTRACT:** Electroreduction of nitrate ( $\text{NO}_3^-$ ) to ammonia ( $\text{NH}_3$ ) is an environmentally friendly route for  $\text{NH}_3$  production, serving as an appealing alternative to the Haber–Bosch process. Recently, various noble metal-based electrocatalysts have been reported for electroreduction of  $\text{NO}_3^-$ . However, the application of pure metal electrocatalysts is still limited by unsatisfactory performance, owing to the weak adsorption of nitrogen-containing intermediates on the surface of pure metal electrocatalysts. In this work, we report thiol ligand-modified Au nanoparticles as the effective electrocatalysts toward electroreduction of  $\text{NO}_3^-$ . Specifically, three mercaptobenzoic acid (MBA) isomers, thiosalicylic acid (ortho-MBA), 3-mercaptopbenzoic acid (meta-MBA), and 4-mercaptopbenzoic acid (para-MBA), were employed to modify the surface of the Au nanocatalyst. During the  $\text{NO}_3^-$  electroreduction, para-MBA modified Au (denoted as para-Au/C) displayed the highest catalytic activity among these Au-based catalysts. At  $-1.0$  V versus reversible hydrogen electrode (vs RHE), para-Au/C exhibited a partial current density for  $\text{NH}_3$  of  $472.2 \text{ mA cm}^{-2}$ , which was 1.7 times that of the pristine Au catalyst. Meanwhile, the Faradaic efficiency (FE) for  $\text{NH}_3$  reached 98.7% at  $-1.0$  V vs RHE for para-Au/C. The modification of para-MBA significantly improved the intrinsic activity of the Au/C catalyst, thus accelerating the kinetics of  $\text{NO}_3^-$  reduction and giving rise to a high  $\text{NH}_3$  yield rate of para-Au/C.

**KEYWORDS:** Ammonia synthesis,  $\text{NO}_3^-$  electroreduction, Au nanoparticles, thiol ligand modification, electronic structure

## INTRODUCTION

As one of the most fundamental industrial products, ammonia ( $\text{NH}_3$ ) is not only an indispensable chemical in fertilizer, medicine, dye, and other industries but also an important carbon-free energy storage medium.<sup>1–3</sup> Currently, the predominant method of  $\text{NH}_3$  synthesis, the Haber–Bosch process, requires extreme reaction conditions of high temperature ( $400\text{--}500$  °C) and high pressure ( $150\text{--}300$  bar) with only 10–20% conversion efficiency.<sup>4–6</sup> It is reported that the annual energy consumption for  $\text{NH}_3$  synthesis accounts for 1–2% of the total global energy supply accompanied by about 1.5% of the global carbon emissions, leading to significant damage to the natural environment.<sup>7–11</sup> Therefore, a clean and economical route for  $\text{NH}_3$  production is urgently needed in pursuit of a sustainable chemical industry.<sup>12–15</sup>

Over the past few decades, the electroreduction of nitrate ( $\text{NO}_3^-$ ) to  $\text{NH}_3$  stands out as one of the desirable pathways for  $\text{NH}_3$  production as an alternative to the Haber–Bosch process.<sup>16–20</sup> Besides, nitrate pollution in water has long been a serious environmental issue all over the world. The high concentration of nitrate in the water body is one of the main reasons for aquatic ecosystem damage and the increase of certain human diseases.<sup>20–22</sup> Utilizing  $\text{NO}_3^-$  as the nitrogen source for  $\text{NH}_3$  synthesis not only satisfies the tremendous

**Received:** November 9, 2023

**Revised:** January 25, 2024

**Accepted:** January 25, 2024

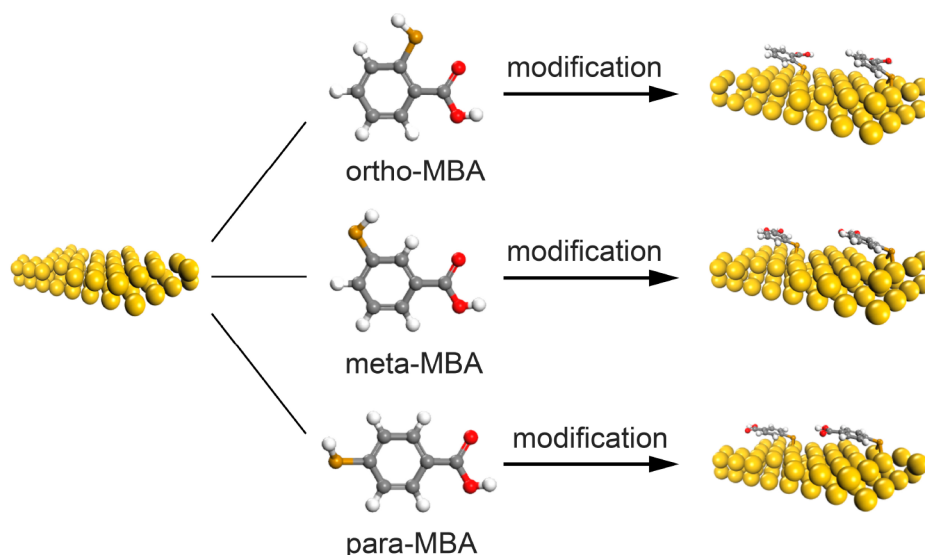


**Figure 1.** Schematic illustration of the synthesis of thiol ligand-modified Au/C. The gold, gray, red, brown, and white spheres represent Au, C, O, S, and H atoms, respectively.

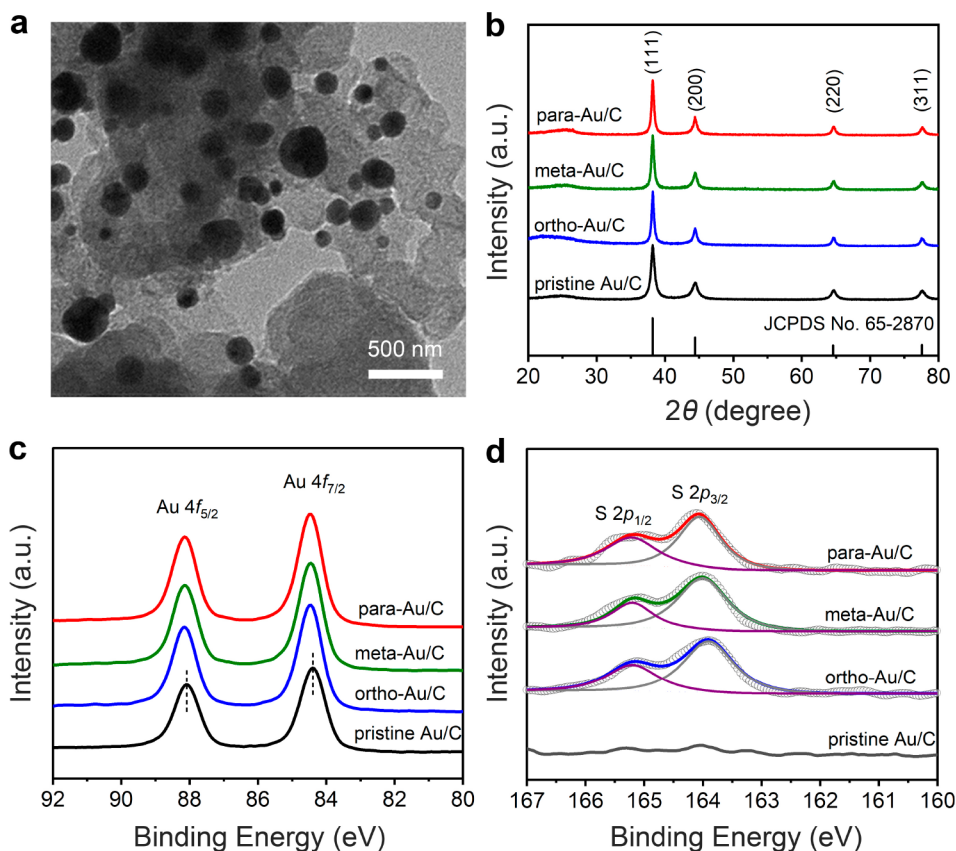


**Figure 2.** (a) TEM image of para-Au/C. (b) XRD, (c) Au 4f XPS, and (d) S 2p XPS of pristine Au/C, ortho-Au/C, meta-Au/C, and para-Au/C.

demand of  $\text{NH}_3$  but also helps mediate the disrupted nitrogen cycle.<sup>3,22</sup> Recently, various metal-based electrocatalysts such as Ir,<sup>23</sup> Pd,<sup>24</sup> Ru,<sup>25</sup> Ag,<sup>26</sup> and Au<sup>27</sup> have been reported for  $\text{NO}_3^-$  electroreduction. However, the application of pure metal electrocatalysts is still limited by unsatisfactory performance owing to the weak adsorption of nitrogen-containing intermediates on the surface of pure metal electrocatalysts.<sup>28,29</sup> Thus, developing an effective method of modulating the electronic structure is crucial to enhancing the intrinsic activity

of pristine catalysts. Among various strategies to manipulate the electronic structures of electrocatalysts, ligand modification is considered especially appealing due to its simplicity and effectiveness in tuning the electronic properties of the catalytic active sites.<sup>30,31</sup> For instance, the ligand X (X = O, OH, F, Cl, Br, and I) axially ligated to Fe- $\text{N}_4$  notably improved the kinetics of the rate-determining step in  $\text{NO}_3^-$  reduction, owing to the change of the  $d$ -band center spin state gap of  $\text{Fe}^{3d}$ .<sup>32</sup> Besides, pyridine functionalization can remarkably augment

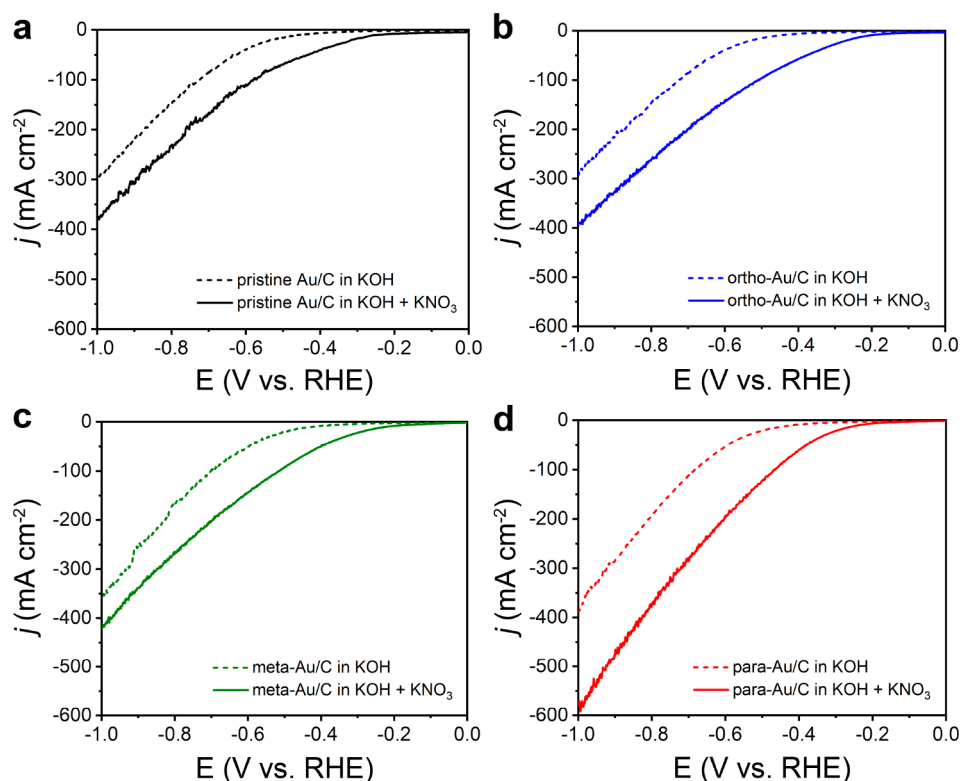


**Figure 3.** LSV of (a) pristine Au/C, (b) ortho-Au/C, (c) meta-Au/C, and (d) para-Au/C in 1.0 M KOH with/without 0.1 M KNO<sub>3</sub> electrolyte.

the activity of Ag nanosheet toward NO<sub>3</sub><sup>−</sup> reduction due to the promoted adsorption of NO<sub>3</sub><sup>−</sup>.<sup>28</sup> As such, it is highly desirable to explore the ligand effect on metal-based catalysts toward the electroreduction of NO<sub>3</sub><sup>−</sup> through the modification of thiol ligands.

In this work, we report a thiol ligand modification method to enhance the performance of Au nanoparticles for the electroreduction of NO<sub>3</sub><sup>−</sup> to NH<sub>3</sub>. We employed three mercaptobenzoic acid (MBA) isomers, including thiosalicylic acid (ortho-MBA), 3-mercaptopbenzoic acid (meta-MBA), and 4-mercaptopbenzoic acid (para-MBA), to modify Au nanoparticles (Figure 1). Para-MBA modified Au catalyst (denoted as para-Au/C) exhibited the best performance among these Au-based catalysts. The partial current density for NH<sub>3</sub> ( $j_{\text{NH}_3}$ ) of para-Au/C reached 472.2 mA cm<sup>−2</sup> with a Faradaic efficiency (FE) up to 98.7% at the potential of −1.0 V versus reversible hydrogen electrode (vs RHE). Besides, the highest yield rate of NH<sub>3</sub> for para-Au/C was 39.7 mg h<sup>−1</sup> cm<sup>−2</sup> at −1.0 V vs RHE, which was 1.7 times that of pristine Au catalyst (denoted as pristine Au/C). The modification of para-MBA significantly improved the intrinsic activity of the Au/C catalyst, thus accelerating the kinetics of NO<sub>3</sub><sup>−</sup> reduction and giving rise to a high NH<sub>3</sub> yield rate of para-Au/C.

## RESULTS AND DISCUSSION

### Synthesis and Characterizations of Thiol-Modified Au Nanoparticles

The Au nanoparticles were fabricated by chemical reduction of HAuCl<sub>4</sub> using NaBH<sub>4</sub>, followed by immobilization on carbon black and soaking in MBA solutions.<sup>33</sup> Au nanoparticles modified by ortho-MBA, meta-MBA, and para-MBA were denoted as ortho-Au/C, meta-Au/C, and para-Au/C, respectively. For comparison, a pristine Au/C catalyst was

prepared in the same process without the soaking step. The transmission electron microscopy (TEM) image of pristine Au/C catalyst clearly depicted the spherical morphology of Au nanoparticles, which were uniformly dispersed on carbon black (Figure S1). After the thiol ligand modification, the morphology and size distribution of ortho-Au/C, meta-Au/C, and para-Au/C displayed no obvious change (Figures 2a, S2, and S3). The X-ray diffraction (XRD) patterns of the catalysts revealed that the metallic Au exhibited a face-centered cubic (fcc) crystal structure with distinct diffraction peaks at 38.2°, 44.4°, 64.6°, and 77.6°, corresponding to the (111), (200), (220), and (311) facets, respectively (Figure 2b).<sup>33</sup> In this case, the phase structure of the Au nanoparticles did not alter significantly after the ligand modification. The high resolution transmission electron microscopy (HRTEM) image of para-Au/C delivered interplanar spacings of 2.36, 2.03, and 1.44 Å, which corresponded to the (111), (200), and (220) facets of Au, respectively (Figure S4a). The selected area electron diffraction (SAED) pattern of para-Au/C exhibited circular rings corresponding to (111), (200), and (222) facets of Au, revealing its polycrystalline nature (Figure S4b). The result of energy-dispersive X-ray spectroscopy (EDS) mapping displayed the uniform distribution of the S element around Au nanoparticles, indicating the accurate attachment of para-MBA to Au atoms in para-Au/C (Figure S5). The X-ray photoelectron spectroscopy (XPS) of Au 4f spectrum of pristine Au/C exhibited two distinct peaks at 84.4 and 88.1 eV, corresponding to 4f<sub>7/2</sub> and 4f<sub>5/2</sub> of metallic Au species, respectively (Figure 2c).<sup>33</sup> Notably, the Au 4f<sub>7/2</sub> XPS peaks of modified Au/C shifted by ~0.05 eV to higher binding energy, which was derived from the electron interaction between Au and S.<sup>34</sup> Moreover, the S 2p XPS spectrum of pristine Au/C showed no signal of S (Figure 2d). In contrast, the modified Au/C revealed two peaks at around 164 and 165 eV,

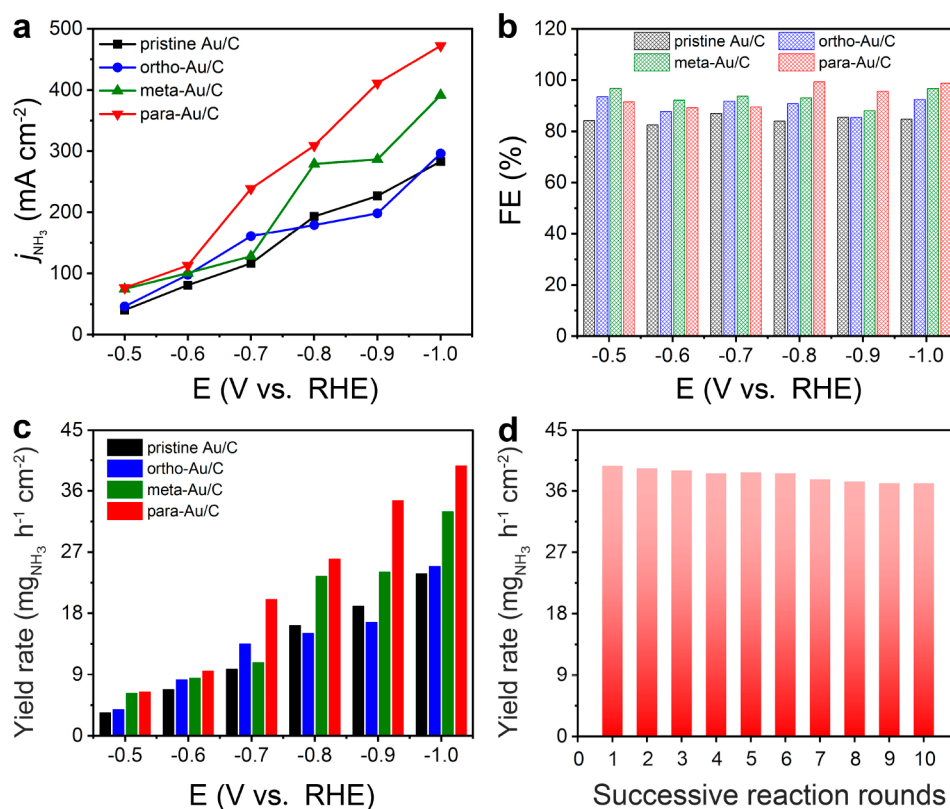


**Figure 4.** (a)  $j_{\text{NH}_3}$ , (b) FE, and (c) yield rate of NH<sub>3</sub> of pristine Au/C, ortho-Au/C, meta-Au/C, and para-Au/C at different applied potentials. (d) The cyclic electrolysis test of para-Au/C at  $-1.0$  V vs RHE.

respectively corresponding to  $S\ 2p_{3/2}$  and  $S\ 2p_{1/2}$  spectra.<sup>36</sup> Compared with the pristine thiol ligands, the shift of  $S\ 2p_{3/2}$  peaks for the modified Au/C catalysts followed the order of para-Au/C > meta-Au/C > ortho-Au/C (Figure S6). In this case, the interaction between Au and S for para-Au/C was the strongest among the modified Au/C catalysts, inducing the strongest regulation of the electronic structure of para-Au/C.

#### Catalytic Performance of NO<sub>3</sub><sup>-</sup> Electroreduction

The electrochemical catalytic performance was measured under ambient conditions in a H-cell. The linear sweep voltammetry (LSV) experiments of Au/C catalysts were conducted in 1.0 M KOH electrolyte with and without 0.1 M KNO<sub>3</sub> (Figure 3). In LSV tests, all four Au/C catalysts delivered much larger current densities in 1.0 M KOH + 0.1 M KNO<sub>3</sub> electrolyte than those in 1.0 M KOH alone at the same potential, suggesting that the kinetics of NO<sub>3</sub><sup>-</sup> electroreduction was much faster than that of H<sub>2</sub> evolution.<sup>35</sup> Besides, the modified Au/C catalysts yielded impressively higher current densities than pristine Au/C, meaning that thiol ligand modification significantly enhanced the catalytic activity of the Au/C catalyst. Among the four catalysts, para-Au/C delivered the highest current density in 1.0 M KOH + 0.1 M KNO<sub>3</sub> electrolyte, implying its highest activity toward NO<sub>3</sub><sup>-</sup> electroreduction. Notably, compared with pristine Au/C, the increment of current densities for para-Au/C in the KOH electrolyte with KNO<sub>3</sub> was considerably greater than those in KOH alone, meaning that the ligand effect had a more pronounced influence on electroreduction of NO<sub>3</sub><sup>-</sup> compared with its impact on H<sub>2</sub> evolution.

To evaluate the catalytic performance of each Au/C catalyst, we conducted electrolysis experiments at different applied

potentials for 1 h. The concentration of NH<sub>3</sub> was determined using the indophenol blue method by UV-vis (Figure S7). Figure 4a illustrates the partial current densities for NH<sub>3</sub> ( $j_{\text{NH}_3}$ ) on four Au/C catalysts. Compared with pristine Au/C, all of the modified Au/C catalysts demonstrated a substantial increment of  $j_{\text{NH}_3}$ . Among these modified catalysts, para-Au/C displayed the highest  $j_{\text{NH}_3}$ , reaching 472.2 mA cm<sup>-2</sup> at the potential of  $-1.0$  V vs RHE. Figure 4b shows the FE for NH<sub>3</sub> of Au/C catalysts during electrolysis. Compared with pristine Au/C, all of the modified catalysts exhibited increased FE for NH<sub>3</sub> production. Especially, para-Au/C displayed a maximal FE of 99.3% at  $-0.8$  V vs RHE. Figure 4c depicts the NH<sub>3</sub> yield rates of Au/C catalysts at different applied potentials. Remarkably, para-Au/C exhibited the highest NH<sub>3</sub> yield rate among the three modified catalysts, reaching 39.7 mg h<sup>-1</sup> cm<sup>-2</sup> at  $-1.0$  V vs RHE. Moreover, the para-Au/C catalyst outperformed most of the reported Au-based electrocatalysts, demonstrating the effectivity of thiol modification as a simple strategy for boosting the catalytic performance (Table S1). Besides, the investigation into the effect of Au loading and soaking time on catalytic performance demonstrated that the optimized Au loading and soaking time were 25 wt % and 1 h, respectively (Figures S8 and S9). The stability test for para-Au/C catalyst was conducted in 1.0 M KOH + 0.1 M KNO<sub>3</sub> electrolyte at  $-1.0$  V vs RHE (Figure 4d). In 10 successive reaction rounds, para-Au/C showed negligible performance degradation, exhibiting only a 6.5% decay for the yield rate of NH<sub>3</sub>. The TEM image and XRD pattern of para-Au/C after cyclic electrolysis displayed no obvious change, representing the structural robustness of para-Au/C (Figure S10). In addition, a <sup>15</sup>N isotope-labeling experiment was conducted to

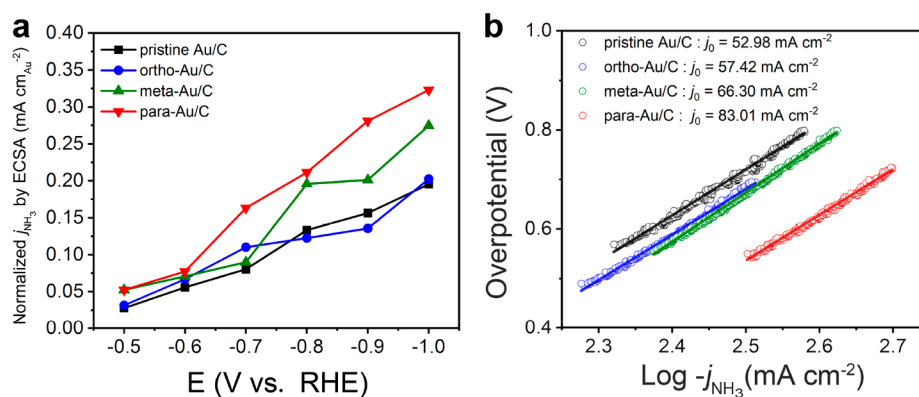


**Figure 5.** (a) ECSA normalized partial current densities for  $\text{NH}_3$ . (b) Tafel plot of pristine Au/C, ortho-Au/C, meta-Au/C, and para-Au/C in 1.0 M KOH with 0.1 M  $\text{KNO}_3$  electrolyte. The  $j_0$  was derived from the intercept of the linear region in Tafel plots.

further quantify the product (Figure S11). The FE for  $\text{NH}_3$  at  $-0.6$  V vs RHE determined by  $^1\text{H}$  NMR was approximated to the results detected via the UV–vis method (Figure S12). These results verified that the generated  $\text{NH}_3$  originated from the electroreduction of  $\text{NO}_3^-$ .

To clarify the intrinsic activity of modified Au/C, the double-layer capacitance ( $C_{\text{dl}}$ ) was measured to calculate the electrochemical active surface areas (ECSAs) of Au/C catalysts.<sup>36</sup> Cyclic voltammetry (CV) of Au/C catalysts was measured at different scan rates, ranging from 20 to 100  $\text{mV s}^{-1}$  (Figure S13). The charging current densities at each scan rate were used to determine the  $C_{\text{dl}}$  of the working electrodes (Figure S14).<sup>37</sup> The  $C_{\text{dl}}$  of pristine Au/C, ortho-Au/C, meta-Au/C, and para-Au/C was calculated to be 11.6, 11.7, 11.4, and 11.7  $\text{mF cm}^{-2}$ , respectively, meaning that the four catalysts had similar ECSAs. Then we normalized the  $j_{\text{NH}_3}$  based on ECSA.<sup>38</sup> As shown in Figure 5a, para-Au/C delivered the highest normalized  $j_{\text{NH}_3}$  among the four Au/C catalysts, indicating that the modification of para-MBA to Au nanoparticles significantly improved the intrinsic activity. Figure S15 displays the electrochemical impedance spectroscopy (EIS) of Au/C catalysts. As shown in the high frequency region of the Nyquist plot, para-Au/C had the lowest charge transfer resistance ( $R_{\text{ct}}$ ) among these Au/C catalysts, suggesting that the charge transfer on para-Au/C was the fastest.<sup>39</sup> To evaluate the kinetics of  $\text{NO}_3^-$  reduction, we calculated the exchange current densities ( $j_0$ ) of each Au/C catalyst based on Tafel plots (Figure 5b). Obviously, the values of  $j_0$  followed the order of para-Au/C > meta-Au/C > ortho-Au/C > pristine Au/C. According to the Butler–Volmer equation, the largest  $j_0$  of para-Au/C represented the fastest kinetics of  $\text{NO}_3^-$  reduction among all four catalysts, thus giving rise to its highest catalytic activity.<sup>40–42</sup> To further elucidate the effect of the ligand on Au/C, density functional theory (DFT) calculations were performed to evaluate the adsorption of  $\text{NO}_3^-$  on pristine Au (111) and para-MBA modified Au (111) (donated as pristine Au and para-Au), respectively (Figure S16). Compared with pristine Au, para-Au exhibited a lower  $\Delta G_{\text{ads}}$  for  $\text{NO}_3^-$ , indicating that para-Au possessed stronger binding with  $\text{NO}_3^-$ . In this case, the boosted catalytic performance of para-Au could be attributed to the facilitated adsorption of  $\text{NO}_3^-$  on the surface of para-Au.

## CONCLUSION

In this work, we developed a simple method of thiol ligand modification to promote the catalytic performance of Au catalyst toward electroreduction of  $\text{NO}_3^-$  to  $\text{NH}_3$ . Among all the modified Au/C catalysts, para-Au/C achieved the  $j_{\text{NH}_3}$  of  $472.2 \text{ mA cm}^{-2}$  with the FE up to 98.7% at the potential of  $-1.0$  V vs RHE. Remarkably, the highest yield rate of  $\text{NH}_3$  for para-Au/C reached up to  $39.7 \text{ mg h}^{-1} \text{ cm}^{-2}$  at  $-1.0$  V vs RHE, which was 1.7 times that of pristine Au/C. Para-MBA modification significantly improved the intrinsic activity of Au/C catalyst, thus accelerating the kinetics of  $\text{NO}_3^-$  reduction and giving rise to the high  $\text{NH}_3$  yield rate of para-Au/C. This work offers an effective chemical modification strategy for guiding the rational design of noble-metal-based electrocatalysts toward  $\text{NO}_3^-$  reduction.

## ASSOCIATED CONTENT

### Supporting Information

The Supporting Information is available free of charge at <https://pubs.acs.org/doi/10.1021/prechem.3c00107>.

Experimental and computational methods; TEM image and size distribution of Au nanoparticles for pristine Au/C, ortho-Au/C, meta-Au/C, and para-Au/C; HRTEM image and EDS mapping of para Au/C; S 2p XPS spectra of ortho-MBA, meta-MBA, and para-MBA; determination of  $\text{NH}_3$  and  $^{15}\text{NH}_3$ ; catalytic performance of para-Au/C with different Au loading and soaking time; CV curves,  $C_{\text{dl}}$ , Nyquist plots for pristine Au/C, ortho-Au/C, meta-Au/C, and para-Au/C; DFT calculation of adsorption for  $^*\text{NO}_3$  on pristine Au and para-Au (PDF)

## AUTHOR INFORMATION

### Corresponding Authors

**Yan Liu** – Hefei National Research Center for Physical Sciences at the Microscale, Key Laboratory of Strongly-Coupled Quantum Matter Physics of Chinese Academy of Sciences, Key Laboratory of Surface and Interface Chemistry and Energy Catalysis of Anhui Higher Education Institutes, Department of Chemical Physics, University of Science and Technology of China, Hefei, Anhui 230026, P. R. China; Email: [yliu1993@ustc.edu.cn](mailto:yliu1993@ustc.edu.cn)

**Zhigang Geng** – Hefei National Research Center for Physical Sciences at the Microscale, Key Laboratory of Strongly-

Coupled Quantum Matter Physics of Chinese Academy of Sciences, Key Laboratory of Surface and Interface Chemistry and Energy Catalysis of Anhui Higher Education Institutes, Department of Chemical Physics, University of Science and Technology of China, Hefei, Anhui 230026, P. R. China; [orcid.org/0000-0003-3183-5900](https://orcid.org/0000-0003-3183-5900); Email: [gengzg@ustc.edu.cn](mailto:gengzg@ustc.edu.cn)

**Jie Zeng** – Hefei National Research Center for Physical Sciences at the Microscale, Key Laboratory of Strongly-Coupled Quantum Matter Physics of Chinese Academy of Sciences, Key Laboratory of Surface and Interface Chemistry and Energy Catalysis of Anhui Higher Education Institutes, Department of Chemical Physics, University of Science and Technology of China, Hefei, Anhui 230026, P. R. China; School of Chemistry & Chemical Engineering, Anhui University of Technology, Ma'anshan, Anhui 243002, P. R. China; [orcid.org/0000-0002-8812-0298](https://orcid.org/0000-0002-8812-0298); Email: [zengj@ustc.edu.cn](mailto:zengj@ustc.edu.cn)

## Authors

**Yuheng Wu** – Hefei National Research Center for Physical Sciences at the Microscale, Key Laboratory of Strongly-Coupled Quantum Matter Physics of Chinese Academy of Sciences, Key Laboratory of Surface and Interface Chemistry and Energy Catalysis of Anhui Higher Education Institutes, Department of Chemical Physics, University of Science and Technology of China, Hefei, Anhui 230026, P. R. China

**Xiangdong Kong** – Hefei National Research Center for Physical Sciences at the Microscale, Key Laboratory of Strongly-Coupled Quantum Matter Physics of Chinese Academy of Sciences, Key Laboratory of Surface and Interface Chemistry and Energy Catalysis of Anhui Higher Education Institutes, Department of Chemical Physics, University of Science and Technology of China, Hefei, Anhui 230026, P. R. China

**Yechao Su** – Hefei National Research Center for Physical Sciences at the Microscale, Key Laboratory of Strongly-Coupled Quantum Matter Physics of Chinese Academy of Sciences, Key Laboratory of Surface and Interface Chemistry and Energy Catalysis of Anhui Higher Education Institutes, Department of Chemical Physics, University of Science and Technology of China, Hefei, Anhui 230026, P. R. China

**Jiankang Zhao** – Hefei National Research Center for Physical Sciences at the Microscale, Key Laboratory of Strongly-Coupled Quantum Matter Physics of Chinese Academy of Sciences, Key Laboratory of Surface and Interface Chemistry and Energy Catalysis of Anhui Higher Education Institutes, Department of Chemical Physics, University of Science and Technology of China, Hefei, Anhui 230026, P. R. China

**Yiling Ma** – Hefei National Research Center for Physical Sciences at the Microscale, Key Laboratory of Strongly-Coupled Quantum Matter Physics of Chinese Academy of Sciences, Key Laboratory of Surface and Interface Chemistry and Energy Catalysis of Anhui Higher Education Institutes, Department of Chemical Physics, University of Science and Technology of China, Hefei, Anhui 230026, P. R. China

**Tongzheng Ji** – Hefei National Research Center for Physical Sciences at the Microscale, Key Laboratory of Strongly-Coupled Quantum Matter Physics of Chinese Academy of Sciences, Key Laboratory of Surface and Interface Chemistry and Energy Catalysis of Anhui Higher Education Institutes, Department of Chemical Physics, University of Science and Technology of China, Hefei, Anhui 230026, P. R. China

**Di Wu** – Hefei National Research Center for Physical Sciences at the Microscale, Key Laboratory of Strongly-Coupled Quantum Matter Physics of Chinese Academy of Sciences, Key Laboratory of Surface and Interface Chemistry and Energy Catalysis of Anhui Higher Education Institutes, Department of Chemical Physics, University of Science and Technology of China, Hefei, Anhui 230026, P. R. China

**Junyang Meng** – Hefei National Research Center for Physical Sciences at the Microscale, Key Laboratory of Strongly-Coupled Quantum Matter Physics of Chinese Academy of Sciences, Key Laboratory of Surface and Interface Chemistry and Energy Catalysis of Anhui Higher Education Institutes, Department of Chemical Physics, University of Science and Technology of China, Hefei, Anhui 230026, P. R. China

Complete contact information is available at:  
<https://pubs.acs.org/10.1021/prechem.3c00107>

## Notes

The authors declare no competing financial interest.

## ACKNOWLEDGMENTS

This work was supported by Strategic Priority Research Program of the Chinese Academy of Sciences (XDB0450401), National Key Research and Development Program of China (2021YFA1500500 and 2019YFA0405600), NSFC (22209161, 22209163, 92061111, 22322901, 22221003, and 22250007), CAS Project for Young Scientists in Basic Research (YSBR-051 and YSBR-022), National Science Fund for Distinguished Young Scholars (21925204), China Post-doctoral Program for Innovative Talents (BX20200324), and Fundamental Research Funds for the Central Universities. J.Z. acknowledges support from the Tencent Foundation through the XPLOER PRIZE. The authors acknowledge support from Prof. Chao Ma and Mr. Sunpei Hu in conducting the microscopic characterization, and Dr. Hong Wu in the DFT computations. This work was partially carried out at the Instruments Center for Physical Science, University of Science and Technology of China. This work was also partially carried out at the USTC Center for Micro and Nanoscale Research and Fabrication.

## REFERENCES

- (1) Chen, J. G.; Crooks, R. M.; Seefeldt, L. C.; Bren, K. L.; Bullock, R. M.; Darensbourg, M. Y.; Holland, P. L.; Hoffman, B.; Janik, M. J.; Jones, A. K.; et al. Beyond fossil fuel-driven nitrogen transformations. *Science* **2018**, *360*, 6391.
- (2) Suryanto, B. H.; Du, H. L.; Wang, D.; Chen, J.; Simonov, A. N.; MacFarlane, D. R. Challenges and prospects in the catalysis of electroreduction of nitrogen to ammonia. *Nat. Catal.* **2019**, *2*, 290–296.
- (3) Chen, F. Y.; Wu, Z. Y.; Gupta, S.; Rivera, D. J.; Lambeets, S. V.; Pecaut, S.; Kim, J. Y. T.; Zhu, P.; Finfrock, Y. Z.; Meira, D. M.; et al. Efficient conversion of low-concentration nitrate sources into ammonia on a Ru-dispersed Cu nanowire electrocatalyst. *Nat. Nanotechnol.* **2022**, *17*, 759–767.
- (4) Inoue, Y.; Kitano, M.; Kishida, K.; Abe, H.; Niwa, Y.; Sasase, M.; Fujita, Y.; Ishikawa, H.; Yokoyama, T.; Hara, M.; Hosono, H. Efficient and stable ammonia synthesis by self-organized flat Ru nanoparticles on calcium amide. *ACS Catal.* **2016**, *6*, 7577–7584.
- (5) Liu, S.; Wang, M.; Qian, T.; Ji, H.; Liu, J.; Yan, C. Facilitating nitrogen accessibility to boron-rich covalent organic frameworks via electrochemical excitation for efficient nitrogen fixation. *Nat. Commun.* **2019**, *10*, 3898.

- (6) Song, Z.; Liu, Y.; Zhao, J.; Zhong, Y.; Qin, L.; Guo, Q.; Geng, Z.; Zeng, J. Promoting N<sub>2</sub> electroreduction into NH<sub>3</sub> over porous carbon by introducing oxygen-containing groups. *Chem. Eng. J.* **2022**, *434*, No. 134636.
- (7) Van der Ham, C. J.; Koper, M. T.; Hettterscheid, D. G. Challenges in reduction of dinitrogen by proton and electron transfer. *Chem. Soc. Rev.* **2014**, *43*, 5183–5191.
- (8) Qing, G.; Ghazfar, R.; Jackowski, S. T.; Habibzadeh, F.; Ashtiani, M. M.; Chen, C. P.; Smith, M. R., III; Hamann, T. W. Recent advances and challenges of electrocatalytic N<sub>2</sub> reduction to ammonia. *Chem. Rev.* **2020**, *120*, 5437–5516.
- (9) Minteer, S. D.; Christopher, P.; Linic, S. Recent developments in nitrogen reduction catalysts: A virtual issue. *ACS Energy Lett.* **2019**, *4*, 163–166.
- (10) Lazouski, N.; Steinberg, K. J.; Gala, M. L.; Krishnamurthy, D.; Viswanathan, V.; Manthiram, K. Proton donors induce a differential transport effect for selectivity toward ammonia in lithium-mediated nitrogen reduction. *ACS Catal.* **2022**, *12*, 5197–5208.
- (11) Kandemir, T.; Schuster, M. E.; Senyshyn, A.; Behrens, M.; Schlögl, R. The Haber-Bosch Process Revisited: On the real structure and stability of “ammonia iron” under working condition. *Angew. Chem., Int. Ed.* **2013**, *52*, 12723–12726.
- (12) Yu, M. S.; Jesudass, S. C.; Surendran, S.; Kim, J. Y.; Sim, U.; Han, M. K. Synergistic interaction of MoS<sub>2</sub> nanoflakes on La<sub>2</sub>Zr<sub>2</sub>O<sub>7</sub> nanofibers for improving photoelectrochemical nitrogen reduction. *ACS Appl. Mater. Interfaces* **2022**, *14*, 31889–31899.
- (13) Kim, D.; Surendran, S.; Janani, G.; Lim, Y.; Choi, H.; Han, M. K.; Yuvaraj, S.; Kim, T. H.; Kim, J. K.; Sim, U. Nitrogen-impregnated carbon-coated TiO<sub>2</sub> nanoparticles for N<sub>2</sub> reduction to ammonia under ambient conditions. *Mater. Lett.* **2022**, *314*, No. 131808.
- (14) Kim, D.; Surendran, S.; Lim, Y.; Choi, H.; Lim, J.; Kim, J. Y.; Han, M. K.; Sim, U. Spinell-type Ni<sub>2</sub>GeO<sub>4</sub> electrocatalyst for electrochemical ammonia synthesis via nitrogen reduction reaction under ambient conditions. *Int. J. Energy Res.* **2022**, *46*, 4119–4129.
- (15) Jeong, Y.; Janani, G.; Kim, D.; An, T. Y.; Surendran, S.; Lee, H.; Moon, D. J.; Kim, J. Y.; Han, M. K.; Sim, U. Roles of heterojunction and Cu vacancies in the Au@Cu<sub>2-x</sub>Se for the enhancement of electrochemical nitrogen reduction performance. *ACS Appl. Mater. Interfaces* **2023**, *15*, 52342–52357.
- (16) Chen, G. F.; Cao, X.; Wu, S.; Zeng, X.; Ding, L. X.; Zhu, M.; Wang, H. Ammonia electrosynthesis with high selectivity under ambient conditions via a Li<sup>+</sup> incorporation strategy. *J. Am. Chem. Soc.* **2017**, *139*, 9771–9774.
- (17) Chen, G. F.; Yuan, Y.; Jiang, H.; Ren, S. Y.; Ding, L. X.; Ma, L.; Wu, T.; Lu, J.; Wang, H. Electrochemical reduction of nitrate to ammonia via direct eight-electron transfer using a copper-molecular solid catalyst. *Nat. Energy* **2020**, *5*, 605–613.
- (18) Li, J.; Zhan, G.; Yang, J.; Quan, F.; Mao, C.; Liu, Y.; Wang, B.; Lei, F.; Li, L.; Chan, A. W.; Xu, L.; et al. Efficient ammonia electrosynthesis from nitrate on strained ruthenium nanoclusters. *J. Am. Chem. Soc.* **2020**, *142*, 7036–7046.
- (19) Sun, W. J.; Ji, H. Q.; Li, L. X.; Zhang, H. Y.; Wang, Z. K.; He, J. H.; Lu, J. M. Built-in electric field triggered interfacial accumulation effect for efficient nitrate removal at ultra-low concentration and electroreduction to ammonia. *Angew. Chem., Int. Ed.* **2021**, *60*, 22933–22939.
- (20) van Langevelde, P. H.; Katsounaros, I.; Koper, M. T. Electrocatalytic nitrate reduction for sustainable ammonia production. *Joule* **2021**, *5*, 290–294.
- (21) Zhang, X.; Wang, Y.; Liu, C.; Yu, Y.; Lu, S.; Zhang, B. Recent advances in non-noble metal electrocatalysts for nitrate reduction. *Chem. Eng. J.* **2021**, *403*, No. 126269.
- (22) Fan, K.; Xie, W.; Li, J.; Sun, Y.; Xu, P.; Tang, Y.; Li, Z.; Shao, M. Active hydrogen boosts electrochemical nitrate reduction to ammonia. *Nat. Commun.* **2022**, *13*, 7958.
- (23) Li, H.; Yan, C.; Guo, H.; Shin, K.; Humphrey, S. M.; Werth, C. J.; Henkelman, G. Cu<sub>x</sub>Ir<sub>1-x</sub> nanoalloy catalysts achieve near 100% selectivity for aqueous nitrite reduction to NH<sub>3</sub>. *ACS Catal.* **2020**, *10*, 7915–7921.
- (24) Lim, J.; Liu, C. Y.; Park, J.; Liu, Y. H.; Senftle, T. P.; Lee, S. W.; Hatzell, M. C. Structure sensitivity of Pd facets for enhanced electrochemical nitrate reduction to ammonia. *ACS Catal.* **2021**, *11*, 7568–7577.
- (25) Gao, W.; Xie, K.; Xie, J.; Wang, X.; Zhang, H.; Chen, S.; Wang, H.; Li, Z.; Li, C. Alloying of Cu with Ru enabling the relay catalysis for reduction of nitrate to ammonia. *Adv. Mater.* **2023**, *35*, No. 2202952.
- (26) Liu, H.; Park, J.; Chen, Y.; Qiu, Y.; Cheng, Y.; Srivastava, K.; Gu, S.; Shanks, B. H.; Roling, L. T.; Li, W. Electrocatalytic nitrate reduction on oxide-derived silver with tunable selectivity to nitrite and ammonia. *ACS Catal.* **2021**, *11*, 8431–8442.
- (27) Yin, H.; Peng, Y.; Li, J. Electrocatalytic reduction of nitrate to ammonia via a Au/Cu single atom alloy catalyst. *Environ. Sci. Technol.* **2023**, *57*, 3134–3144.
- (28) Yang, H. Y.; He, K. Y.; Ai, X.; Liu, X.; Yang, Y.; Yin, S. B.; Jin, P. J.; Chen, Y. Pyridine functionalized silver nanosheets for nitrate electroreduction. *J. Mater. Chem. A* **2023**, *11*, 16068–16073.
- (29) Liu, J. X.; Richards, D.; Singh, N.; Goldsmith, B. R. Activity and selectivity trends in electrocatalytic nitrate reduction on transition metals. *ACS Catal.* **2019**, *9*, 7052–7064.
- (30) Cheng, R.; Min, Y.; Li, H.; Fu, C. Electronic structure regulation in the design of low-cost efficient electrocatalysts: From theory to applications. *Nano Energy* **2023**, *115*, No. 108718.
- (31) Abeyweera, S. C.; Yu, J.; Perdew, J. P.; Yan, Q.; Sun, Y. Hierarchically 3D porous Ag nanostructures derived from silver benzenethiolate nanoboxes: Enabling CO<sub>2</sub> reduction with a near-unity selectivity and mass-specific current density over 500 A/g. *Nano Lett.* **2020**, *20*, 2806–2811.
- (32) Huang, Y.; Tang, C.; Li, Q.; Gong, J. Computational studies for boosting nitrate electroreduction activity of Fe-N<sub>4</sub>-C Single-Atom catalyst via axial fifth ligand. *Appl. Surf. Sci.* **2023**, *616*, No. 156440.
- (33) Gao, D.; Zhang, Y.; Zhou, Z.; Cai, F.; Zhao, X.; Huang, W.; Li, Y.; Zhu, J.; Liu, P.; Yang, F.; Wang, G.; Bao, X. Enhancing CO<sub>2</sub> electroreduction with the metal-oxide interface. *J. Am. Chem. Soc.* **2017**, *139*, 5652–5655.
- (34) Battocchio, C.; Porcaro, F.; Mukherjee, S.; Magnano, E.; Nappini, S.; Fratoddi, I.; Quintiliani, M.; Russo, M. V.; Polzonetti, G. Gold nanoparticles stabilized with aromatic thiols: Interaction at the molecule-metal interface and ligand arrangement in the molecular shell investigated by SR-XPS and NEXAFS. *J. Phys. Chem. C* **2014**, *118*, 8159–8168.
- (35) Li, L.; Tang, C.; Cui, X.; Zheng, Y.; Wang, X.; Xu, H.; Zhang, S.; Shao, T.; Davey, K.; Qiao, S. Z. Efficient nitrogen fixation to ammonia through integration of plasma oxidation with electrocatalytic reduction. *Angew. Chem., Int. Ed.* **2021**, *133*, 14250–14256.
- (36) Song, Z.; Liu, Y.; Zhong, Y.; Guo, Q.; Zeng, J.; Geng, Z. Efficient electroreduction of nitrate into ammonia at ultralow concentrations via an enrichment effect. *Adv. Mater.* **2022**, *34*, No. 2204306.
- (37) Song, Z.; Qin, L.; Liu, Y.; Zhong, Y.; Guo, Q.; Geng, Z.; Zeng, J. Efficient electroreduction of nitrate to ammonia with CuPd nanoalloy catalysts. *ChemSusChem* **2023**, *16*, No. e202300202.
- (38) Yoon, Y.; Yan, B.; Surendranath, Y. Suppressing Ion Transfer Enables Versatile Measurements of Electrochemical Surface Area for Intrinsic Activity Comparisons. *J. Am. Chem. Soc.* **2018**, *140*, 2397–2400.
- (39) Niu, Z.; Fan, S.; Li, X.; Wang, P.; Liu, Z.; Wang, J.; Bai, C.; Zhang, D. Bifunctional copper-cobalt spinel electrocatalysts for efficient tandem-like nitrate reduction to ammonia. *Chem. Eng. J.* **2022**, *450*, No. 138343.
- (40) Costa, G. F.; Pinto, M. R.; Messias, I.; Junior, J.; Singh, N.; Nagao, R. Tracking copper oxidation state during nitrate electrochemical reduction reaction. *Meet. Abstr.* **2023**, *MA2023-01*, 2300.
- (41) De, D.; Englehardt, J. D.; Kalu, E. E. Electroreduction of nitrate and nitrite ion on a platinum-group-metal catalyst-modified carbon fiber electrode chronoamperometry and mechanism studies. *J. Electrochem. Soc.* **2000**, *147*, 4573.

(42) Albery, W. J. Electrode kinetics. *Philos. Trans. R. Soc. London A*  
**1981**, *302*, 221–235.